Compact Modeling of STT-MTJ for SPICE Simulation

Zihan Xu, *Ketul B. Sutaria*, *Chengen Yang*, *Chaitali Chakrabarti*, *Yu Cao*
School of Electrical, Computer and Energy Engineering, Arizona State University
Tempe, Arizona 85287, USA
Email: {zihanxu, kbsutari, chengen.yang, chaitali, ycao}@asu.edu

***Abstract*—STT-MTJ is a promising device for future high-density and low-power integrated systems. To enable design exploration of STT-MTJ, this paper presents a fully compact model for efficient SPICE simulation. Derived from the fundamental LLG equation, the new model consists of RC elements that are *closed-form* solutions of device geometry and material properties. They support transient SPICE simulations, providing necessary details beyond the macromodel. The accuracy is validated with numerical results and published data.**

INTRODUCTION

As Si technology is scaling toward the 10nm regime, CMOS-based devices may no longer be the technology of choice. Instead, emerging devices, such as spin-transfer torque (STT) based magnetic tunnel junction (MTJ), are more scalable and are viable alternatives for both memory and logic design in the post-silicon era [1][2]. Indeed, STT-MTJ promises a good combination of high density, fast access, low switching power, and non-volatile data storage [3]. Figure 1 illustrates the basic structure and the switching behavior of a STT-MTJ device [4]. By programming it with a current pulse, the magnetic moment in the free layer can be switched to be 0^o (parallel, *P*) or 180^o (anti-parallel, *AP*) to that in the fixed layer. This is the essential process to define the digital state.

To explore the design potential of STT-MTJ, compact modeling is a critical bridge between the underlying technology and large-scale design practice. This compact model should be fully *compatible* with the SPICE simulator, such that designers can mix STT-MTJ with CMOS devices to realize new functions. It should be *scalable* with process and operation conditions, capturing all *dynamic* and static properties during the operation. Furthermore, the new compact model should have high simulation *efficiency*, which is important for statistical design of memory applications.

Such a model is presented in this paper. Previous approaches either only address the macromodel [4], which lacks sufficient flexibility and switching details, or still use complicated equations and iterations in SPICE simulation [3]. Our work transfers the fundamental Landau-Lifshitz-Gilbert (LLG) equation into a passive RC network, in which all components are closed-form solutions of device geometry and material properties. As demonstrated in Fig.1, the new SPICE model efficiently generates the transient behavior under all programming conditions. The physical basis of model derivation further helps gain design insights on STT-MTJ.

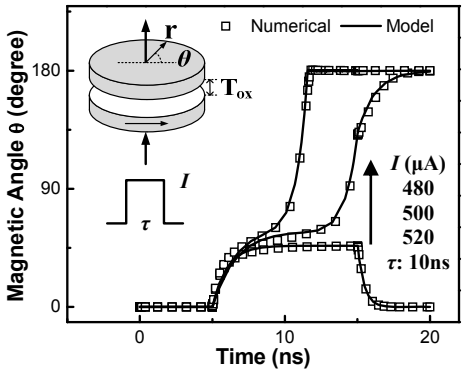

Figure 1. An in-plane STT-MTJ is programmed by a current pulse. The magnitude (I) and the width (τ) of the current pulse determine the switching success of the magnetic angle (θ) in the free layer.

COMPACT MODELING OF STT-MTJ

The modeling focus is to solve the LLG equation into an equivalent RC network, for all possible switching conditions.

A. STT-MTJ Basics

Figure 1 shows the three layers in STT-MTJ at the radius r and the dielectric thickness T_{ox}. The magnetic moment ($\vec{M}$) of one layer is free while the other is fixed. With I, the spin of the electrons is polarized by the fixed layer, and transferred to the free layer. The state of *P* or *AP* affects MTJ resistance [1]. The dynamics of $\vec{M}$ is defined by the LLG equation [5][6]:

$$\frac{d\vec{M}}{dt} = -\gamma\mu_0\vec{M}\times\vec{H}_{eff} - \gamma\frac{2K}{M_s^2}\left(\vec{M}\cdot\vec{u}_{ea}\right)\cdot\left(\vec{M}\times\vec{u}_{ea}\right) + \frac{\alpha}{M_s}\vec{M}\times\frac{d\vec{M}}{dt} + \eta\frac{\mu_B I}{eV} \quad (1)$$

The terms (from left to right) represent the Zeeman torque, by both the local field and the thermal fluctuation field, the anisotropic torque, the damping torque, and the spin-transfer torque, in which the efficiency (η) depends on the current direction. Table I defines key model parameters.

TABLE I. PARAMETERS ON THE GEOMETRY AND MATERIALS.

Saturation magnetization (M_s)	$M_{s0}\left[4\left(1-\frac{1}{4r/ch-1}\right)\cdot\exp\left(-\frac{2S_b}{3R}\frac{1}{4r/ch-1}\right)-3\right]$ [7]	
Effective magnetic field ($\vec{H}_{eff}$)	Intrinsic $\vec{H}$ +thermal fluctuation $\vec{H}_f$ [6]	
Gyromagnetic ratio (γ)	Anisotropic const. (K)	Damping const. (α)
$1.76\text{x}10^{11}$ rad·s^{-1}/T	$1.13\text{x}10^5$ T·A/m	0.02

B. Dynamic Magnetization Model

The switching of the magnetic moment is the key dynamics in STT-MTJ. In general, it is a three dimensional movement: the Zeeman torque and the anisotropic torque contribute to the rotation in the plane perpendicular to the easy axis, indicated by an angle φ; the damping torque and the spin-transfer torque dominate the switching in the easy plane, resulting in the change of θ. Considering a realistic structure of STT-MTJ (Fig. 1), the change of the magnetic moment can be separated into two planes and thus, the LLG equation reduced to two scalar equations of magnetic angle φ and θ.

$$M_s \frac{d\varphi}{dt} = -\gamma\mu_0 M_s H \sin\theta - 2\gamma K \sin\theta\cos\theta \tag{2}$$

$$M_s \frac{d\theta}{dt} = \alpha M_s \frac{d\varphi}{dt} + \eta\frac{\mu_B I}{eV} \tag{3}$$

Substituting $d\varphi/dt$ from Eq. (2) to Eq. (3):

$$M_s \frac{d\theta}{dt} = -\alpha\gamma\left(\mu_0 M_s H \sin\theta + 2K\sin\theta\cos\theta\right) + \eta\frac{\mu_B I}{eV} \tag{4}$$

The scalar equation of Eq. (4) is the foundation to analyze the switching dynamics of θ. Based on Eq. (4), Fig. 2 plots $d\theta/dt$ for different I when θ changes from 0° to 180°. Some critical points are highlighted below in order to obtain the physical map for further model derivation:

- Threshold current (I_{th}): This concept separates two possible switching mechanisms in a STT-MTJ device, precession switching and thermally assisted switching. When $I > I_{th}$, $d\theta/dt$ is always > 0 (Fig. 2) and thus, the magnetic angle is able to complete the switching with sufficient τ. However, when $I < I_{th}$, $d\theta/dt$ may be < 0, requiring the assist of thermal fluctuation H_f to statistically switch STT-MTJ [8]. As the thermal process takes a longer time and is not deterministic, today's STT-MTJ usually follows the precession switching. I_{th} can be solved from the minimum of $d\theta/dt$ = 0, which is associated with the threshold angle θ_{th} (Fig. 2).

- Critical angle (θ_c): This angle defines a critical value the magnetic moment has to reach at the end of the current pulse; if θ at time = τ is smaller than θ_c, the damping torque may pull θ_c back to 0° (Fig. 1). As observed in Fig. 2, when I = 0, there are three points to satisfy $d\theta/dt$ = 0: 0° and 180° are two stable solutions, while θ_c is a metastable point. This behavior is similar as that in a SRAM cell, and helps us develop the model of θ_c.

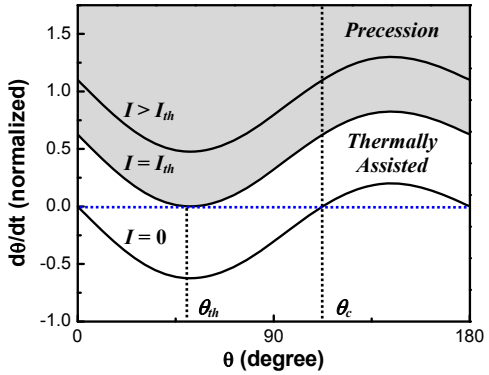

Figure 2. The critical concepts during the switching.

TABLE II. MODELS OF CRITICAL POINTS ($P \rightarrow AP$).

θ_{th}	$\cos^{-1}\left[\left(\sqrt{(\mu_0 M_s H)^2 + 32K^2} - \mu_0 M_s H\right)\Big/(8K)\right]$
I_{th}	$\alpha\gamma(eV)/\eta\mu_B \cdot \left[\mu_0 M_s H \sin\theta_{th} + K\sin(2\theta_{th})\right]$
θ_c	$\cos^{-1}\left[-\mu_0 M_s H/(2K)\right]$
I_c	$(\pi r^2)\cdot\left(2.1\times10^{-4} M_s/\tau + 0.34 M_s H + 4.26\times10^{10}\right)$

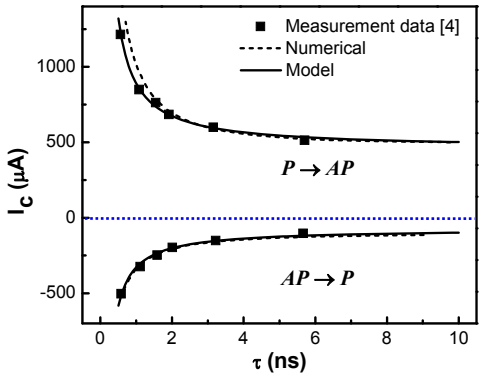

Figure 3. Validation with published STT-MTJ data [4]. (r = 45nm, T_{ox} = 0.85nm)

- Critical current (I_c): Given the pulse width τ, I_c is the minimum current required to switch the magnetic angle from 0° to θ_c. $I > I_c$ ensures a successful precession switching. To solve I_c, Eq. (4) is integrated from 0° to θ_c for dθ, and from 0 to τ for dt. A compact solution is obtained (Table II). I_c is proportional to the inverse of τ, implying a tradeoff between speed and the writing power in design optimization.

Table II summarizes the models for $P \rightarrow AP$, in standard international units. For $AP \rightarrow P$, the formulas remain the same, but with different coefficient values due to the different initial condition. The formulas in Table II have a clear root in physics, and are accurate in the precession switching. They are scalable with process and material parameters, supporting the development of the RC network in Section III. Figure 3 validates our model with the measurement data [4]. Due to the operation nature of STT-MTJ, it requires more current and energy to switch it from P to AP (Fig. 3).

C. TMR Model of the Tunnel Junction

The switching of the magnetic angle represents the write process of STT-MTJ. The read of the state is by characterizing the resistance of MTJ. When a read current is delivered to STT-MTJ, the resistance reaches a low value (R_P) if the magnetic moments in both ferromagnetic layers are in parallel; otherwise a higher resistance (R_{AP}) is detected. Coupled with the dynamic magnetization procedure in previous section, this property completes the operation of STT-MTJ.

The tunnel magneto-resistance (TMR) of MTJ is defined as (R_{AP}-R_P)/R_P. During the continuous switching of the magnetic angle, the change of MTJ resistance follows [9]:

$$R(\theta) = 2R_P\left(\frac{1+TMR}{2+TMR+TMR\cdot\cos\theta}\right) \tag{5}$$

The static values of R_{AP} and R_P are calculated from the tunneling current through T_{ox} [9]. Eq. (5) is used to model the dynamic resistance during the switching period.

SPICE IMPLEMENTATION

The details of the switching period are important for various design purpose, such as power and yield [3]. In addition, design applications of STT-MTJ usually involve CMOS as the control device. For these reasons, compact model of STT-MTJ needs to be embedded into the SPICE simulator. Different from previous approach that directly implement the LLG equation through complex Verilog-A codes [3][4], this work proposes a simple RC network that is physical, intuitive, and general.

D. Regional RC Structure for Circuit Simulation

Starting from the fundamental LLG equation (Eq. (4)), sinθ can be approximated as θ, 1, or -θ, when θ is close 0^o, 90^o, or 180^o, respectively. A similar treatment can be applied to cosθ. By expanding sinθ and cosθ in this approach, $d\theta/dt$ in Eq. (4) is expressed as a linear function of θ, and thus, the solution of the LLG equation is transferred as a passive RC network for SPICE simulation.

Based on this general principle, four distinct regions are recognized, easing the implementation. Figure 4 shows the network which supports transient SPICE simulations, with the output node representing θ. *R*s are functions of those critical points in Table II, and *C* is a constant, as derived below:

- *Region I*: This is at the beginning of the current pulse, when θ is close to 0 and thus, sinθ~θ and cosθ~1. The damping torque resists the change of θ, implying that the R_1C network is a negative feedback. V_1, which is a linear function of applied *I*, is charging the output node.

- *Region 2*: As soon as θ exceeds the threshold angle θ_{th}, θ is close to 90^o so that sinθ~1 and cosθ~90^o-θ. In this region, $d^2\theta/dt^2$ becomes positive, as indicated in Fig. 2. Such a fact suggests that the RC network is a positive feedback: the increase in θ helps speed up the switching. Therefore, a negative resistance, R_2, is obtained from Eq. (4), giving an exponential increase in the magnetic angle (Fig. 4). If the current pulse stays long enough, the magnetic angle rapidly reaches 180^o, as shown in Fig. 1. However, if τ is not long enough to complete the switching, two more regions are needed for time > τ.

- *Region 3*: If $\theta > \theta_c$ when the current pulse ends, the damping torque helps finish the switching without *I*, as shown in Figs. 1 and 5. In this case, Eq. (4) can be expanded around 180^o to obtain R_3C.

- *Region 4*: Finally, if $\theta < \theta_c$ when the current pulse ends, the damping torque overwhelms and pulls the magnetic angle back to the initial state, 0^o. The switching fails, under the influence of R_4C.

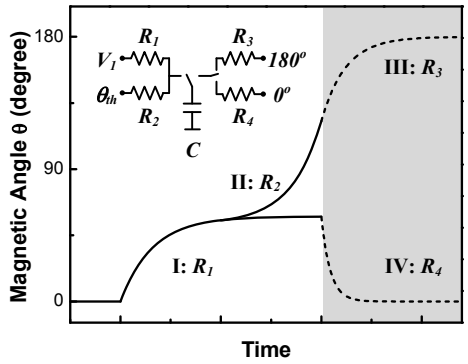

Figure 4. The regional RC network for dynamic SPICE simulation.

TABLE III. FORMULAS FOR THE RC ELEMENTS IN SPICE.

V_1	$\theta_{th} + a(I - I_{th})/(\pi r^2)$
R_1	$K_1(\mu_0 M_s H + 2K)/M_s$
R_2	$K_2[1 - b(I - I_{th})/(\pi r^2)]K/M_s$
R_3	$K_3(2K - \mu_0 M_s H)$
R_4	$K_4(\mu_0 M_s H + 2K)/M_s$

Table III summarizes all model parameters. They are in closed-form, derived from the LLG equation and parameters in Table II. The proposed RC network is followed by the *TMR* model (Eq. (5), in Verilog-A) to complete the simulation structure. Working together, they convert the magnetic angle to electrical resistance. As all parameter values are pre-solved before the simulation, this RC network is highly efficient in the SPICE environment.

E. Demonstration of the SPICE Model

The newly developed models are implemented into SPICE. Two simulation examples are presented in Figs. 1 and 3. Under the same assumptions of *I*, *r* and T_{ox}, Fig. 5 further demonstrates the prediction under different pulse width τ. As expected by the RC network in Fig. 4, different RC components are activated, depending on the switching

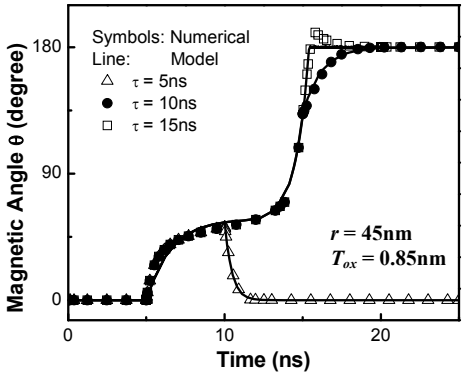

Figure 5. The switching behavior under different pulse widths.

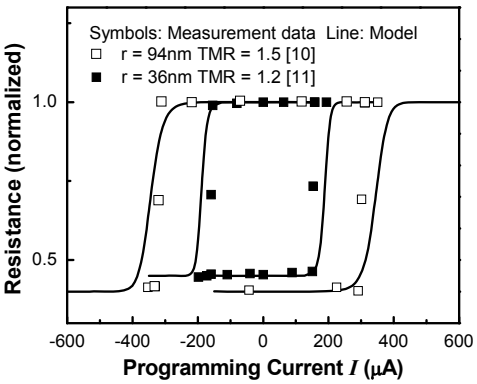

Figure 6. The matching in the prediction of MTJ resistance.

condition. The success of data writing is determined by both the magnitude and the duration of the current pulse. The proposed modeling and simulation method smoothly captures such a behavior for design exploration.

By combining the switching model and the *TMR* model together, the new solution generates the electrical property of STT-MTJ. Figure 6 validates this approach with the experimental data [10][11]. For a STT-MTJ device, since $P \rightarrow AP$ starts from $\theta = 0^o$ but $AP \rightarrow P$ starts from $\theta = 180^o$, these two switching paths experience different switching thresholds, as predicted by the LLG equation. This causes the hysteresis behavior in the resistance, which is well matched by our proposed models. In addition, the new compact model is general enough to describe the data from different processes, as demonstrated in Fig. 6.

DESIGN BENCHMARKING

With solid validation with numerical results and published data, the proposed compact model enables all types of design exploration with STT-MTJ. Under the shrinking of device feature size, Fig. 7 shows the minimum programming current, I_c. The radius r impacts the density of I_c mainly through saturation magnetization (M_s in Table I), which is a material property [7]. The density of I_c is sensitive to r only when $r <$ 20nm. On the contrary, I_c is highly sensitive to T_{ox}, as T_{ox} affects the intrinsic magnetic field in Eq. (1). In addition, T_{ox} has a strong influence on the resistance and the long-term reliability of the tunnel junction [9]. Thus, process control of T_{ox} is extremely important to STT-MTJ based memory design.

From the perspective of design optimization, Fig. 8 investigates the energy consumption during the write process. When the current pulse is narrow for high-speed operations, I_c is high for a successful switching and thus, the energy consumption is high. As τ increases, I_c goes down, reducing the energy cost. However, I_c becomes less sensitive to τ after $\tau >$ 5ns and the energy consumption increases again even with a wider pulse, because of the longer integration time. As observed in Fig. 8, for a low-power design, there exists an optimal programming current that achieves minimum energy consumption of the write process, at $\tau \sim$ 3ns.

SUMMARY

STT-MTJ represents a promising alternative for future logic and memory applications. Compact modeling of STT-MTJ is essential for integrated design, performance analysis and optimization. Unique from previous approaches on macro-modeling or direct implementation of the LLG equation, this work proposes a set of closed-form solutions, which map the physics of the LLG equation into a RC network. The values of RCs are pre-solved from the geometry, material properties, and the appropriate switching region. The new approach supports SPICE simulation with high efficiency, paving the path for further design study of STT-MTJ.

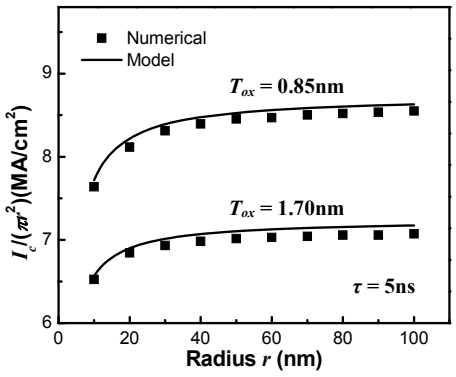

Figure 7. The new model is sensitive to process parameters.

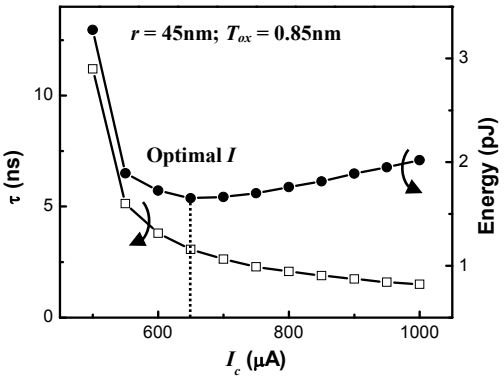

Figure 8. There is an optimal I for minimum energy consumption.

ACKNOWLEDGEMENT

This research is sponsored by National Science Foundation (NSF) under CNS-1218183.

REFERENCES

[1] X. Wang, Y. Chen, H. Li, D. Dimitrov, H. Liu, "Spin torque random access memory down to 22nm technology," *Trans. Magn*., vol. 44, no. 11, pp. 2479-2482, Nov. 2008.

[2] M. Sharad, C. Augustine, G. Panagopoulos, K. Roy, "Spin-based neuron model with domain-wall magnets as synapse," *Trans. Nanotechnology*, vol. 11, no. 4, pp. 843-853, Jul. 2012.

[3] P. Wang, W. Zhang, R. Joshi, R. Kanj, Y. Chen, "A thermal and process variation aware MTJ switching model and its applications in soft error analysis," *ICCAD*, pp. 720-727, 2012.

[4] K. C. Chun, J. Zhao, J. D. Harms, T.-H. Kim, J.-P. Wang, C. H. Kim, "A scaling roadmap and performance evaluation of in-plane and perpendicular MTJ based STT-MRAMs for high-density cache memory," *JSSC*, vol. 48, no. 2, pp. 598-610, Feb. 2013.

[5] D. C. Ralph, M. D. Stiles, "Current perspectives: Spin transfer torques," *J. MMM*, vol. 320, pp. 1190-1216, Mar. 2008.

[6] J.-B. Kammerer, M. Madec, L. Hébrard, "Compact modeling of a magnetic tunnel junction – Part I: Dynamic magnetization model," *TED*, vol. 57, no. 6, pp. 1408-1415, Jun. 2010.

[7] H. M. Lu, W. T. Zheng, Q. Jiang, "Saturation magnetization of ferromagnetic and ferrimagnetic nanocrystals at room temperature," *J. Phys. D: Appl. Phys*., vol. 40, pp. 320-325, Jan. 2007.

[8] L.-B. Faber, W. Zhao, J.-O. Klein, T. Devolder, C. Chappert, "Dynamic compact model of spin-transfer torque based magnetic tunnel junction (MTJ)," *DTIS*, pp. 130-135, 2009.

[9] M. Madec, J.-B. Kammerer, L. L. Hébrard, "Compact modeling of a magnetic tunnel junction – Part II: Tunneling current model," *TED*, vol. 57, no. 6, pp. 1416-1424, Jun. 2010.

[10] Z. Diao *et al*., "Spin-transfer torque switching in magnetic tunnel junctions and spin-transfer torque random access memory," *J. Phys.: Condensed Matter*, vol. 19, no. 16, Apr. 2007.

[11] C. J. Lin *et al*., "45nm low power CMOS logic compatible embedded STT MRAM utilizing a reverse-connection 1T/1MTJ cell," *IEDM*, pp. 11.6.1-11.6.4, 2009.